Environmental Science & Technology

pubs.acs.org/est

Article

Reactivity of Dissolved Organic Matter with the Hydrated Electron: Implications for Treatment of Chemical Contaminants in Water with Advanced Reduction Processes

Benjamin D. Fennell, Douglas Fowler, Stephen P. Mezyk,* and Garrett McKay*

Cite This: *Environ. Sci. Technol.* 2023, 57, 7634−7643

Read Online

ACCESS | Metrics & More | Article Recommendations | Supporting Information

ABSTRACT: Advanced reduction processes (ARP) have garnered increasing attention for the treatment of recalcitrant chemical contaminants, most notably per- and polyfluoroalkyl substances (PFAS). However, the impact of dissolved organic matter (DOM) on the availability of the hydrated electron (e_{aq}^-), the key reactive species formed in ARP, is not completely understood. Using electron pulse radiolysis and transient absorption spectroscopy, we measured bimolecular reaction rates constant for e_{aq}^- reaction with eight aquatic and terrestrial humic substance and natural organic matter isolates (k_{DOM,e_{aq}^-}), with the resulting values ranging from (0.51 ± 0.01) to (2.11 ± 0.04) × 10^8 M_C^{-1} s^{-1}. k_{DOM,e_{aq}^-} measurements at varying temperature, pH, and ionic strength indicate that activation energies for diverse DOM isolates are ≈18 kJ mol^{-1} and that k_{DOM,e_{aq}^-} could be expected to vary by less than a factor of 1.5 between pH 5 and 9 or from an ionic strength of 0.02 to 0.12 M. k_{DOM,e_{aq}^-} exhibited a significant, positive correlation to % carbonyl carbon for the isolates studied, but relationships to other DOM physicochemical properties were surprisingly more scattered. A 24 h UV/sulfite experiment employing chloroacetate as an e_{aq}^- probe revealed that continued e_{aq}^- exposure abates DOM chromophores and e_{aq}^- scavenging capacity over a several hour time scale. Overall, these results indicate that DOM is an important e_{aq}^- scavenger that will reduce the rate of target contaminant degradation in ARP. These impacts are likely greater in waste streams like membrane concentrates, spent ion exchange resins, or regeneration brines that have elevated DOM concentrations.

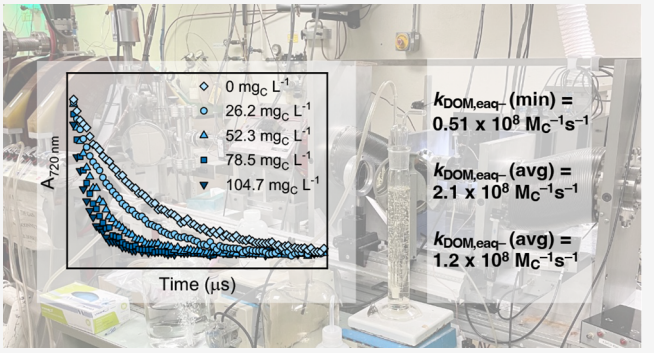

KEYWORDS: *dissolved organic matter, hydrated electron, kinetics, electron pulse radiolysis, reducing moieties*

1. INTRODUCTION

Dissolved organic matter (DOM) is a complex, heterogeneous mixture of organic compounds naturally occurring in surface waters and groundwaters.[1] DOM acts as a radical scavenger, thereby lowering the concentration of reactive species available for target contaminant degradation in advanced oxidation processes (AOP)[2,3] and advanced reduction processes (ARP).[4−6] Reactions between DOM and oxidizing radicals have been well characterized in the context of AOP, including hydroxyl radicals ($^{\bullet}OH$),[7,8] sulfate radicals ($SO_4^{\bullet-}$),[9] carbonate radicals ($CO_3^{\bullet-}$),[10] chlorine radicals ($Cl^{\bullet}$ and $Cl_2^{\bullet-}$),[11] and bromine radicals ($Br^{\bullet}$ and $Br_2^{\bullet-}$).[12] In ultraviolet-advanced reduction processes (UV-ARP), the hydrated electron (e_{aq}^-) is considered to be the main reducing species[4,5,13−15] with an aqueous reduction potential of −2.9 V.[16] However, despite the growing interest in e_{aq}^--mediated contaminant degradation, the reactivity of e_{aq}^- with DOM is not well understood.

The scavenging of e_{aq}^- by DOM represents an intrinsic limitation for the application of ARP in contaminated waters. ARP have been shown to degrade recalcitrant contaminants such as bromate,[15,17−22] halogenated organic compounds,[4,13,14,23−31] and per- and polyfluoroalkyl substances (PFAS),[32−42] but the majority of these studies have been performed in relatively clean systems (e.g., lab-grade water). Some studies have tested ARP for treating concentrated waste streams produced from membrane filtration reject[42] or regeneration of adsorbents,[43] which have elevated DOM concentrations. Ren et al. also demonstrated that increasing the concentration of Aldrich humic acid inhibited the

Received: February 2, 2023
Revised: April 17, 2023
Accepted: April 18, 2023
Published: May 4, 2023

https://doi.org/10.1021/acs.est.3c00909
Environ. Sci. Technol. 2023, 57, 7634−7643

degradation of perfluorooctanoic acid in the UV/sulfite system.[6] Another study conducted by Duan and Batchelor showed inhibited perchlorate degradation with increasing DOM concentration in the UV/sulfite ARP.[44] As noted in these studies, and in parallel to the UV-AOP literature, this inhibition of target contaminant degradation can occur by DOM shielding the e_{aq}^- sensitizer from absorbing UV photons, by scavenging e_{aq}^-, or by a combination of both processes. While the impact of light screening can be predicted based on absorbance measurements,[45] accurate predictions of e_{aq}^- scavenging by DOM are limited by the lack of reported bimolecular rate constants for this reaction.

The objectives of this study were to evaluate how the reactivity of e_{aq}^- with DOM depends on DOM physicochemical properties, environmental conditions, and the prolonged e_{aq}^- exposure typically encountered in ARP systems. These objectives were accomplished by quantifying bimolecular reaction rate constants (k_{DOM,e_{aq}^-}) using electron pulse radiolysis for eight humic substance and natural organic matter (NOM) isolates in buffered solution at neutral pH and measuring k_{DOM,e_{aq}^-} values as a function of pH, ionic strength, and temperature for selected DOM samples. The isolates employed represent a wide range of physiochemical properties and chemical composition, being derived from both terrestrial and aquatic sources.[46] Insights into the variability of k_{DOM,e_{aq}^-} among samples were gleaned by evaluating correlations to the physicochemical properties of DOM. Lastly, the impact of prolonged e_{aq}^- exposure on DOM-e_{aq}^- scavenging was evaluated in a 24 h UV/sulfite experiment conducted with Suwanee River natural organic matter II. Results from this study provide a means for estimating the e_{aq}^- scavenging capacity of DOM in ARP, informing how this scavenging capacity changes with environmental conditions, and indicate that e_{aq}^- scavenging by DOM can impact the efficacy of target contaminant degradation even after significant e_{aq}^- exposure.

2. MATERIALS AND METHODS

2.1. DOM Isolates, Chemicals, and Sample Preparation. Chemicals were purchased from Sigma-Aldrich or VWR and are listed in Table S1 in the Supporting Information (SI). In addition, eight humic substance and natural organic matter (NOM) isolates were purchased from the International Humic Substances Society (IHSS) and used for electron pulse radiolysis experiments, including Elliott Soil humic acid IV (ESHA IV), Pahokee Peat fulvic acid II (PPFA II), Pahokee Peat humic acid I (PPHA I), Pony Lake fulvic acid (PLFA), Suwannee River fulvic acid II (SRFA II), Suwannee River humic acid II (SRHA II), Suwannee River natural organic matter II (SRNOM II), and Upper Mississippi River natural organic matter (MRNOM). The IHSS catalog number for each isolate is available in SI Table S2. Additional IHSS catalog numbers were used for optical measurements (see SI Table S3) and k_{DOM,e_{aq}^-} comparison (SI Tables S5−S8), including Suwannee River fulvic acid III (SRFA III), Suwannee River humic acid III (SRHA III), and Elliott Soil humic acid V (ESHA V). All DOM stock solutions were prepared at a concentration of 200 mg L^{-1} in 10 mM dibasic phosphate that was adjusted to pH 5, 7, or 9 using $HClO_4$, HCl, or NaOH. $HClO_4$ was used for the pulse radiolysis studies. Ionic strength was varied using $NaClO_4$. Ultrapure water (≥18.2 MΩ·cm) used for all experiments was obtained from either the Notre Dame University Radiation Laboratory reverse osmosis water treatment system or a Barnstead purification system (Thermo Fisher).

2.2. Analytical Measurements. Analytical measurements included pH, absorbance, dissolved organic carbon (DOC), and anion analysis. pH measurements were made with either an Orion Research pH/millivolt meter 811 (Notre Dame Radiation Laboratory) or a Thermo Scientific Orion Versa Star Pro combined with a micro Mettler Toledo LE422 pH probe (Texas A&M). A Cary-100 spectrophotometer (Agilent) with a 1 cm pathlength quartz cuvette was used to measure absorbance spectra, which were used to calculate specific ultraviolet absorbance at 254 nm ($SUVA_{254}$) and spectral slope ($S_{300-600}$) for the isolates. SI Text S1 provides additional measurement and calculation details for $SUVA_{254}$ and $S_{300-600}$. DOC measurements were performed by Hazen Huffman Laboratories in Golden, Colorado. Prior to DOC analysis, samples were acidified with trace-metal-grade nitric acid (70%) to pH ≤ 2.0 and stored at 4 °C. Anion analysis, except for sulfite, was conducted on a Dionex Integrion ion chromatography system equipped with a conductivity detector, a Dionex IonPac AS19 column (4 mm × 250 mm), a Dionex IonPac AG19 (4 mm × 50 mm) guard column, and a Dionex ADRS 600 (4 mm) suppressor. Anions were eluted with 20 mM KOH at a 1.0 mL min^{-1} flow rate and a 50 mA suppressor current. The column was temperature-controlled at 30 °C. Sulfite concentrations were quantified using the 5,5′-dithiobis-(2-nitrobenzoic acid) assay and a thiol molar absorption coefficient of 14,000 M^{-1} cm^{-1}, as described previously.[47,48]

2.3. Electron Pulse Radiolysis Techniques. k_{DOM,e_{aq}^-} values were measured using the linear accelerator system at the University of Notre Dame Radiation Laboratory.[49] Numerous studies have utilized this approach to quantify bimolecular rate constants for reactions between organic compounds and various radical species.[50−54] Methods previously established and utilized in this study for bimolecular reaction rate determination are briefly discussed below.

DOM stock solutions (200 mg L^{-1}) were diluted with phosphate buffer in one of two dilution series (series 1: 160, 120, 80, and 40 mg L^{-1}; series 2: 150, 100, and 50 mg L^{-1}) in quartz cuvettes, purged with argon gas for at least 2 min, and sealed with glass stoppers. Water radiolysis via 7 ns electron pulses yielded 0.27 μmol e_{aq}^- per J of energy absorbed.[16] The transient e_{aq}^- decays were monitored at 720 nm on a microsecond time scale for the dilution series as well as a phosphate buffer blank (DOM at 0 mg L^{-1}) also purged with argon. Transient decay traces were averaged (~30 traces) and fit with a first-order exponential decay plus baseline model to extract the pseudo-first-order decay constants of e_{aq}^- (k'), which were then plotted vs the DOM concentration to obtain k_{DOM,e_{aq}^-}. In this analysis, the change in k' is due solely to the change in DOM concentration because the scavenging capacity of the background solvent is constant. Bimolecular rate constants were normalized to carbon concentration using the carbon mass % provided by the IHSS.[55] Additional details involving pulse radiolysis techniques are discussed in SI Text S2.

2.4. Photochemical Irradiation Experiments. Irradiation experiments were conducted in duplicate immersion well reactors (Ace Glass) with an exterior glass body and interior quartz sleeve. Reactors were filled with ultrapure water (~590 mL) and 1.0 mM borate buffer (pH 10.0) and purged with

https://doi.org/10.1021/acs.est.3c00909
Environ. Sci. Technol. 2023, 57, 7634−7643

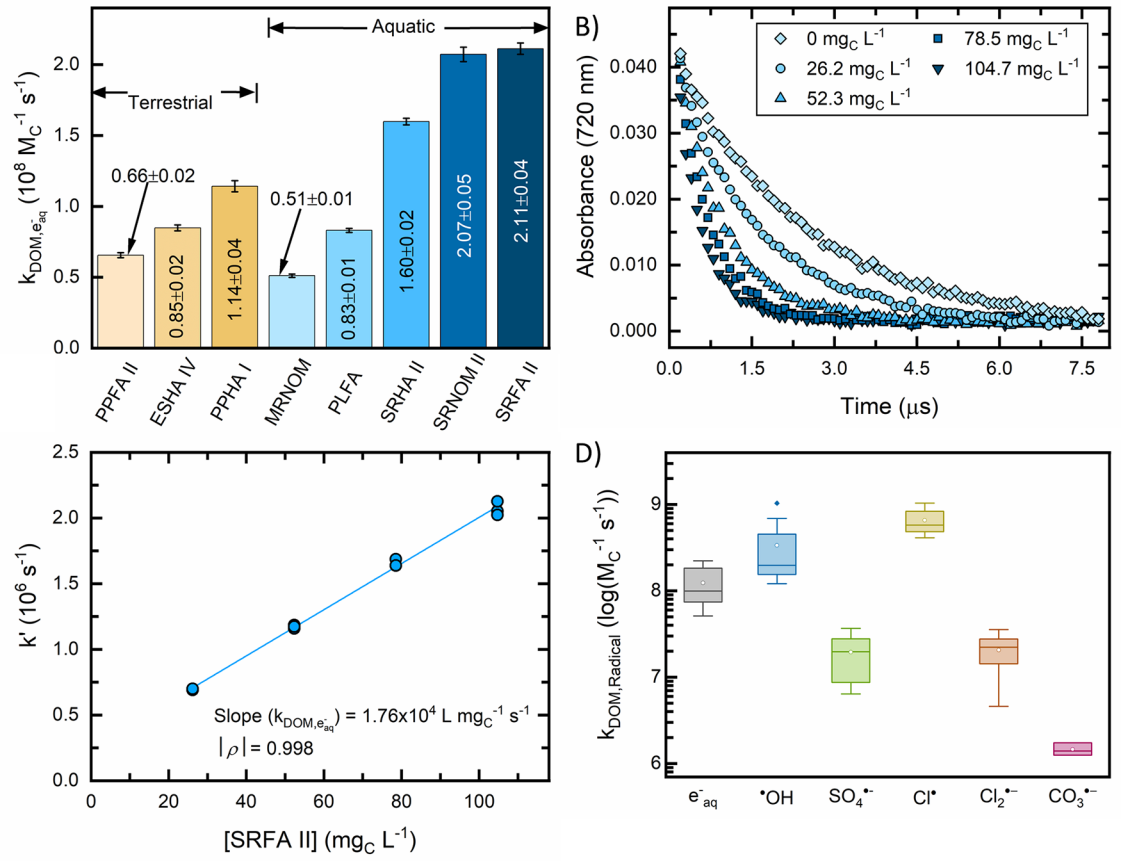

Figure 1. Bimolecular rate constant measurements between e_{aq}^- and DOM isolates (k_{DOM,e_{aq}^-}). Isolates include Elliott Soil IV humic acid (ESHA IV), Pahokee Peat II fulvic acid (PPFA II), Pahokee Peat I humic acid (PPHA I), Upper Mississippi River natural organic matter (MRNOM), Pony Lake fulvic acid (PLFA), Suwannee River II humic acid (SRHA II), Suwannee River II natural organic matter (SRNOM II), and Suwannee River II fulvic acid (SRFA II). k_{DOM,e_{aq}^-} in (A) were determined by measuring (B) transient absorption decay kinetics of e_{aq}^- at 720 nm for various [DOM] and plotting (C) pseudo-first-order rate constant as a function of [DOM]. (B, C) Data for SRFA II only. The solid line in (C) represents a linear fit to the data using the least squares method with the slope reported as the k_{DOM,e_{aq}^-}. Similar (C) plots for other DOM isolates are found in SI Figure S1. Error bars in (A) represent the standard error of the slope in (C). k_{DOM,e_{aq}^-} were compared to bimolecular rate constants between other radicals[7−11] and DOM isolates in (D). DOM-e_{aq}^- experiments conducted at pH 7.0 ± 0.1, 22 ± 2 °C, and 10.0 mM phosphate buffer. All other radical experiments in (D) were conducted at pH 7.0, room temperature, and varying concentrations of phosphate buffer.

nitrogen gas for at least 45 min prior to and during experiments. The temperature in the reactors was controlled at 20 °C using a recirculating chiller. A low-pressure Hg, non-ozone forming lamp (10 W LSE Lighting GPH212T5L/4P) was powered on for at least 15 min and briefly turned off before concentrated stock solutions of sulfite, SRNOM II, and monochloroacetic acid (MCAA) were added to the reactor. UV/sulfite experiments were performed at a pH at least 2 pH units above the pK_a of HSO_3^- (pK_a = 7.2) and under anerobic conditions to minimize e_{aq}^- scavenging impacts of HSO_3^-, H^+, and O_2.[16,45,56,57] After spiking, the solution was mixed for at least 30 s and stirring was maintained throughout experiments using a magnetic stir bar at 400 rpm. Experiments were initiated by turning on the lamps and collecting aliquots of solution using a stainless-steel needle and syringe. Samples were collected in either falcon tubes or 1.5 mL polypropylene vials and stored at 4 °C before analysis. UV irradiance was measured as 1.26×10^{-8} Es cm^{-2} s^{-1} using uridine actinometry[58] and the previously measured average reactor pathlength was determined as 2.23 cm using the H_2O_2 method.[47,59,60]

3. RESULTS AND DISCUSSION

3.1. DOM Isolate and e_{aq}^- Bimolecular Rate Constant Measurements. k_{DOM,e_{aq}^-} values at pH 7.0 and 22 ± 2 °C varied by approximately a factor of 4, ranging from (0.51 ± 0.01) to (2.11 ± 0.04) × 10^8 M_C^{-1} s^{-1} (Figure 1A). k_{DOM,e_{aq}^-} values were determined by finding the pseudo-first-order rate constant from the transient e_{aq}^- decay data (Figure 1B) and plotting the pseudo-first-order rate constant against the DOM concentration (Figure 1C). A linear fit to the data in Figure 1C yields k_{DOM,e_{aq}^-} as the slope with the *y*-intercept representing any e_{aq}^- scavengers other than DOM (e.g., H^+ in acidic conditions) present in the background solvent (see SI Text S2 for additional discussion). SI Figure S1 contains similar pseudo-first-order plots for the other DOM isolates and SI Text S3 discusses the minimal impact of IHSS catalog number on DOM-specific k_{DOM,e_{aq}^-} values.

k_{DOM,e_{aq}^-} values for soil humic substance isolates ranged from (0.66 ± 0.02) × 10^8 M_C^{-1} s^{-1} (PPFA II) to (1.14 ± 0.04) × 10^8 M_C^{-1} s^{-1} (PPHA I) and largely overlap with those of aquatic isolates, which ranged from (0.51 ± 0.01) × 10^8 M_C^{-1}

https://doi.org/10.1021/acs.est.3c00909
Environ. Sci. Technol. 2023, 57, 7634−7643

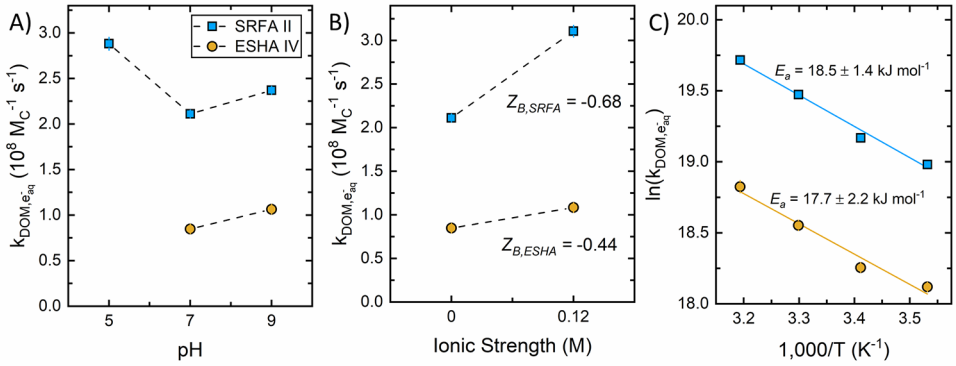

Figure 2. Influence of (A) pH, (B) ionic strength, and (C) temperature on bimolecular rate constants for SRFA II and ESHA IV. Experiments conducted at 22 ± 2 °C, pH 7.0 ± 0.1, and 10.0 mM dibasic phosphate buffer unless otherwise specified. The Z_B in (B) was calculated from the Brønsted-Bjerrum equation (eq 3.1) using the charge of e_{aq}^- (i.e., $Z_A = -1$). Error bars represent the standard error of the bimolecular rate constant (majority of error bars are within markers). Additional plots of the pseudo-first-order rate constant against the DOM concentration for each pH, temperature, and ionic strength condition are provided in SI Figures S3 and S4.

s^{-1} (MRNOM) to (2.11 ± 0.04) × 10^8 M_C^{-1} s^{-1} (SRFA II). Soil humic acid k_{DOM,e_{aq}^-} values were lower than that for SRHA II, an aquatic humic acid. The k_{DOM,e_{aq}^-} value for PPFA II, a terrestrial fulvic acid, was also lower than the k_{DOM,e_{aq}^-} for SRFA II, an aquatic fulvic acid. However, not all k_{DOM,e_{aq}^-} values for aquatic isolates were higher than isolate terrestrial k_{DOM,e_{aq}^-} values. For example, MRNOM and PFLA (aquatic origin) had lower k_{DOM,e_{aq}^-} values than PPHA I (soil origin). Isolates from the Suwannee River had the largest k_{DOM,e_{aq}^-} values, with SRFA II and SRNOM II exhibiting similar reactivity and SRHA II being ~20% lower. Overall, while k_{DOM,e_{aq}^-} is variable among these DOM samples, there is no clear trend between isolation procedure (humic substance *vs* natural organic matter) or source (aquatic *vs* soil).

The range of k_{DOM,e_{aq}^-} values reported on an M_C^{-1} s^{-1} basis falls within the range of bimolecular reaction rate constants reported in the literature for oxidizing radicals' reaction with DOM (Figure 1D and SI Table S4).[7−11] On average, k_{DOM,e_{aq}^-} values were exceeded only by $^{\bullet}OH$ and $Cl^{\bullet}$ values. DOM is a primary sink for oxidizing radicals in sunlit waters and advanced oxidation processes. In anaerobic systems, such as electron transfer in anaerobic bottom waters and sediments or engineered systems like ARP, DOM will be an important e_{aq}^- scavenger. Based on an average of the values measured for humic substance and NOM isolates, we recommend a k_{DOM,e_{aq}^-} value of 1.2 × 10^8 $M_C^{-1}s^{-1}$ (1.0 × 10^4 L mg_C^{-1} s^{-1}). Employing this value yields an e_{aq}^- scavenging capacity of 1.0 × 10^5 s^{-1} at a dissolved organic carbon concentration of 10 mg_C L^{-1}.

3.2. Impact of pH, Temperature, and Ionic Strength on k_{DOM,e_{aq}^-}. We evaluated the impact of pH, temperature, and ionic strength on k_{DOM,e_{aq}^-} for two isolates, SRFA II and ESHA IV (Figure 2). Increasing pH from 7 and 9 caused small but significant increases in k_{DOM,e_{aq}^-} for both ESHA IV and SRFA II (Figure 2A, between 1.1- and 1.3-fold). Conversely, increasing pH from 5 and 7 caused a 1.4-fold decrease in k_{DOM,e_{aq}^-} for SRFA II.

The impact of pH on k_{DOM,e_{aq}^-} may be attributed to changes in the reactivity of DOM moieties at different protonation states, the impact of ionization on DOM molecular size, and the accessibility of reducible moieties to e_{aq}^-. Protonation of carboxylic acids generally increases the e_{aq}^- bimolecular rate constant (e.g., acetic acid, $k = 2 \times 10^8$ M^{-1} s^{-1}; acetate, $k < 1 \times 10^6$ M^{-1} s^{-1}).[16] This could explain the decrease in k_{DOM,e_{aq}^-} for SRFA II between pH 5 and 7 (we were unable to measure k_{DOM,e_{aq}^-} at pH 5 for ESHA IV). Increasing pH from 7 to 9 results in a greater fraction of ionized phenolic moieties, which have a lower reactivity than their corresponding protonated species. However, phenol is much less reactive with e_{aq}^- ($k = 2 \times 10^7$ M^{-1} s^{-1})[16] compared to carboxylic acids. Increasing protonation of phenols and carboxylic acids with decreasing pH lowers the DOM charge density,[61] making the reaction of e_{aq}^- with DOM more favorable from an electrostatic perspective. A competing effect is the impact of ionization state on DOM size. As the pH increases, electrostatic repulsion between negatively charged DOM moieties intensifies, resulting in molecular expansion[62] and easier access to the reducible DOM moieties (e_{aq}^- is formed in the aqueous phase upon absorption of radiation). Thus, the slight increase in k_{DOM,e_{aq}^-} between pH 7 and 9 is consistent with an increase in accessibility of e_{aq}^- to reducible DOM moieties.

The ionic strength trend observed for both SRFA II and ESHA IV at pH 7 behaved according to the Brønsted-Bjerrum equation, eq 3.1, (i.e., the rate constant for like-charged reactants increases with increasing ionic strength).

$$\log\left(\frac{k_{2,I}}{k_{2,I=0}}\right) = 1.02 Z_A Z_B \frac{\sqrt{I}}{1+\sqrt{I}} \tag{3.1}$$

In eq 3.1, $k_{2,I}$ represents the bimolecular rate constant at ionic strength I, $k_{2,I=0}$ represents the bimolecular rate constant at infinite dilution, and Z_AZ_B is the product of the charges of the reactants. We approximated $k_{2,I=0}$ with k_{DOM,e_{aq}^-} values measured in 10 mM phosphate buffer (I = 0.02 M at pH 7). Due to the negative charge of e_{aq}^-, a higher ionic strength results in a shielding of the like-charged reactants, directly decreasing the coulombic repulsion forces and increasing reactivity with anionic species. This shielding effect was observed for both SRFA II and ESHA IV when ionic strength was increased (Figure 2B) but to slightly different extents, with k_{DOM,e_{aq}^-} increasing by 1.3-fold for ESHA IV and 1.5-fold for SRFA II.

https://doi.org/10.1021/acs.est.3c00909
Environ. Sci. Technol. 2023, 57, 7634−7643

Table 1. k_{DOM,e_{aq}^-} Values and Characterization Data for Humic Substance and NOM Isolates

sample[a]	$SUVA_{254}$[b,c] ($L\ mg_C^{-1}\ m^{-1}$)	$S_{300-600}$[b] (nm^{-1})	H/C[d]	O/C[d]	% aromatic[e]	% carbonyl[e]	M_nQ[d] (charge $molecule^{-1}$)	k_{DOM,e_{aq}^-}[f] ($10^8\ M_C^{-1}\ s^{-1}$)	k_{DOM,e_{aq}^-}[f] ($10^4\ L\ mg_C^{-1}\ s^{-1}$)
ESHA IV[b]	7.4	0.0074	0.05	0.54	41	1	10.8	0.85 ± 0.02	0.71 ± 0.02
PPFA II	5.9	0.0134	0.07	0.84	39	3.6	14.7	0.66 ± 0.02	0.55 ± 0.01
PPHA I	6.1	0.0090	0.07	0.66	47	5	12.4	1.14 ± 0.04	0.95 ± 0.03
PLFA	1.2	0.0170	0.10	0.60	12	1.2	3.20	0.83 ± 0.01	0.69 ± 0.01
SRFA II[b]	4.3	0.0158	0.08	0.82	22	5	7.98	2.11 ± 0.04	1.76 ± 0.03
SRHA II[b]	5.1	0.0124	0.08	0.80	31	6	10.4	1.60 ± 0.02	1.33 ± 0.02
SRNOM II	3.2	0.0146	0.08	0.82	23	8	8.64	2.07 ± 0.05	1.73 ± 0.04
MRNOM	2.8	0.0147	0.09	0.83	19	3	9.61	0.51 ± 0.01	0.43 ± 0.01

[a]Experiments conducted at standard conditions of 22 ± 2 °C, pH 7.0 ± 0.1, and 10.0 mM dibasic phosphate buffer unless otherwise specified. [b]IHSS catalog numbers vary for $SUVA_{254}$ and $S_{300-600}$ values. See SI Table S3. [c]Values based on [DOC] calculated from isolate mass per volume normalized to IHSS percent carbon. [d]Values unavailable for DOM isolates prepared in nonstandard conditions. [e]Values listed here are significant figures reported on the IHSS website.[66] [f]Average k_{DOM,e_{aq}^-} value is 1.22 ± 0.63 × $10^8\ M_C^{-1}\ s^{-1}$ or 1.02 ± 0.53 × $10^4\ L\ mg_C^{-1}\ s^{-1}$.

One possible explanation is that, at pH 7 and high ionic strength, DOM structures have expanded such that the reducible moieties are more accessible to e_{aq}^- and some negatively charged DOM moieties have been shielded. This explanation is consistent with the abovementioned impact of increasing pH from 7 to 9 for these same isolates. Furthermore, using the Brønsted-Bjerrum equation, we calculated the Z_B value, using a (−1) charge for e_{aq}^-.[16] The calculated Z_B values for SRFA II and ESHA IV were −0.68 and −0.44, respectively, which is much less negative than DOM charge density values reported based on other methods.[63] One possibility is that negatively charged moieties are spatially distant from the site of e_{aq}^- reaction. Another explanation is that increasing DOM charge impacts DOM's three-dimensional structure and that the subsequent effect on k_{DOM,e_{aq}^-} is not fully captured by eq 3.1. Future research measuring k_{DOM,e_{aq}^-} under a greater range of pH values and ionic strength conditions could help discern among these possibilities.

Activation energies (E_a) for the reaction of e_{aq}^- with SRFA II and ESHA IV at pH 7 were calculated using the measured temperature-dependent k_{DOM,e_{aq}^-} values and the Arrhenius equation (eq 3.2)

$$\ln(k_{DOM,e_{aq}^-}) = -\frac{E_a}{R}\frac{1}{T} + \ln(A) \tag{3.2}$$

where A is the Arrhenius pre-factor, R is the gas constant, and T is the temperature (K). Plotting ln (k_{DOM,e_{aq}^-}) against 1000/T yields a slope $-E_a/R$ from which E_a was determined (Figure 2C). The activation energies for SRFA II and ESHA IV were the same within error (18.5 ± 1.4 and 17.7 ± 2.2 kJ mol^{-1}, respectively), suggesting that an average E_a of 18 kJ mol^{-1} can generally be applied to assess the temperature dependence of e_{aq}^- scavenging by DOM in ARP systems.

3.3. Relationships between Bimolecular Rate Constants and DOM Composition. We investigated correlations between the measured k_{DOM,e_{aq}^-} values and DOM physiochemical properties to provide clues to the factors governing the reactivity of DOM with e_{aq}^-. Physicochemical properties included elemental ratios (H/C and O/C), $SUVA_{254}$, $S_{300-600}$, carbon distribution from ^{13}C NMR, and number-average molecular charge (M_nQ). These physicochemical properties for each DOM isolate along with the respective k_{DOM,e_{aq}^-} values are shown in Table 1 for standard experimental conditions (pH 7.0, 10 mM phosphate buffer, 22 ± 2 °C). Elemental ratios and carbon distributions were taken from the IHSS website for each isolate's catalog number, M_nQ was taken from previous studies,[64,65] and $SUVA_{254}$ and $S_{300-600}$ were measured in this study. Additional information about measurement and calculation of the DOM physicochemical properties and k_{DOM,e_{aq}^-} values under nonstandard conditions are provided in the Supporting Information (Texts S4 and S5 and Tables S7−S9).

Of the physicochemical properties examined, k_{DOM,e_{aq}^-} had the strongest relationship with the % carbonyl carbon as determined by ^{13}C NMR. The positive linear correlation between k_{DOM,e_{aq}^-} and % carbonyl carbon (ρ = 0.809) was statistically significant (p = 0.0046) (Figure 3A) and is consistent with the known high reactivity of e_{aq}^- with carbonyl compounds.[16] For example, a sampling of literature bimolecular e_{aq}^- rate constants for model organic compounds shows that carbonyl-containing compounds exhibit consistently higher reactivity than other functional groups (Figure 3B).

The lack of strong correlations between k_{DOM,e_{aq}^-} and other DOM physicochemical properties (e.g., % aromaticity, M_nQ) was surprising given the known impact of charge and functional group on the reactivity of model organic compounds with e_{aq}^-. For example, we hypothesized that k_{DOM,e_{aq}^-} would tend to decrease with increasing DOM negative charge (M_nQ), but this was not observed (see SI Figure S5). Similarly, we expected k_{DOM,e_{aq}^-} to be positively correlated to the electron accepting capacity,[68] but this was also not observed (see SI Figure S5). In comparison, recent reports of bimolecular rate constants for oxidizing radicals such as $SO_4^{\bullet-}$ and halogen radicals ($X^\bullet$ and $X_2^{\bullet-}$) with DOM have yielded significant correlations with DOM physicochemical properties such as $SUVA_{254}$ and electron donating capacity.[9,11,12] Bimolecular rate constants for DOM with $^\bullet OH$ have not been described by a single parameter; rather multiple linear regression models or principal component analysis has been employed.[51,69] Preliminary attempts were made in this study to correlate groups of 7−9 parameters, but these attempts only confirmed that % carbonyl carbon was the most significant predictor of k_{DOM,e_{aq}^-}. These statistical analyses may prove useful in future studies on the reactivity of DOM with e_{aq}^- but will require a larger sample set than analyzed here.

Overall, the lack of correlations between k_{DOM,e_{aq}^-} and DOM physicochemical properties observed herein indicates that k_{DOM,e_{aq}^-} is not governed by a single aspect of DOM's

https://doi.org/10.1021/acs.est.3c00909
Environ. Sci. Technol. 2023, 57, 7634−7643

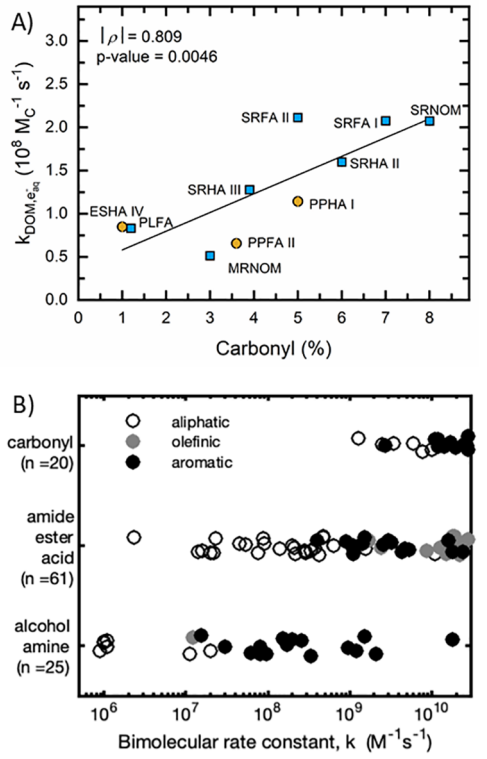

Figure 3. Relationships between DOM composition and e_{aq}^- bimolecular rate constant. (A) Correlation k_{DOM,e_{aq}^-} and % carbonyl carbon as determined by ^{13}C NMR and reported by the IHSS. Markers refer to values derived from the slope of first-order rate constants vs [DOM] (e.g., Figure 1C), and error bars refer to the standard error of the slope (majority of error bars are within markers). Marker color represents terrestrial (brown) and aquatic isolates (blue). SRNOM data represent SRNOM I for carbonyl % and SRNOM II for k_{DOM,e_{aq}^-}. All other IHSS catalog numbers match exactly. Experiments conducted at 22 ± 2 °C, pH 7.0 ± 0.1, and 10.0 mM dibasic phosphate buffer. (B) Bimolecular rate constants between model organic compounds and e_{aq}^- from literature sources (accessed via https://kinetics.nist.gov/solution/).[67]

composition. It is likely, however, that aquatic-based DOM will have a larger impact on e_{aq}^- scavenging in ARP treatment due to the presence of a higher % carbonyl carbon.

3.4. Comparison of Organic Model Compounds and DOM Reaction with e_{aq}^-. Prior studies of radical reactions ($^{\bullet}OH$, $SO_4^{\bullet-}$, $X^{\bullet}$ and $X_2^{\bullet-}$; $X = Cl^-$, Br^-) with DOM have shown that measured rate constants can be reasonably well predicted using an average value of individual reacting components chosen to represent DOM composition.[7,9,11,12] To test this hypothesis for e_{aq}^- reaction, a set of model compounds with known e_{aq}^- bimolecular rate constants were selected based on prior compilations for oxidizing radicals,[7,9,11,12] and the below equation was applied (eq 3.3)

$$k_{DOM,e_{aq}^-} = \sum_i \alpha_i k_i \tag{3.3}$$

where α_i and k_i are the fractional contribution and bimolecular rate constant (units of $M_C^{-1}s^{-1}$) of model organic compound *i*. α_i was varied across the three scenarios listed below to evaluate the range of possible % aromatic and % carbonyl carbon present in these isolates.

Scenario 1: Each model compound is set to an equal concentration resulting in 49.2% aromatic carbon and 5.3% carbonyl carbon. A 49.2% aromatic carbon is higher than aquatic isolates but only slightly higher than soil humic acids.

Scenario 2: The % aromatic carbon was chosen to be 20% and is partitioned equally between the aromatic compounds in the model compound set. The α_i for acetone is set to 0.07 and the remaining α_i's are distributed equally among methyl acetate, *tert*-butanol, and alanine.

Scenario 3: The % aromatic carbon was set to 40% and α_i for acetone is set to 0. The high aromatic % and low carbonyl % for this scenario are representative of characterization data for ESHA IV and V.

Contrary to the good agreement observed in previous studies for DOM reactions with oxidizing radicals,[7,9,11,12] the three scenarios tested all resulted in k_{DOM,e_{aq}^-} values that were either at the upper end or exceeded k_{DOM,e_{aq}^-} values measured by pulse radiolysis (Table 2). The lower measured k_{DOM,e_{aq}^-} values could be the result of geometric effects (reactive e_{aq}^- moieties are not accessible to radiolytically formed e_{aq}^-), charge impacts (DOM typically exhibits a large negative charge, which may slow down k_{DOM,e_{aq}^-} relative to singly charged organic compounds), or a combination of these factors. Future research is needed to discern among these possibilities.

3.5. Impact of DOM on e_{aq}^- Exposure during the UV/Sulfite ARP. The measured k_{DOM,e_{aq}^-} values indicate that DOM will be an important scavenger of e_{aq}^- in ARP. In treatment technologies in which e_{aq}^- is formed photochemically, DOM

Table 2. Summary of Results from Applying Eq 3.3 to Predict Hydrated Electron Rate Constants for DOM Using Model Compounds

model compound data[a]				scenario 1		scenario 2		scenario 3	
compound	formula	k (10^7 M^{-1} s^{-1})	k (10^7 M_C^{-1} s^{-1})	α_i	$\alpha_i k_i$	α_i	$\alpha_i k_i$	α_i	$\alpha_i k_i$
phenol	C_6H_6O	2.00	0.33	0.11	0.037	0.04	0.01	0.08	0.03
2-hydroxybenzoate	$C_7H_6O_3$	1000	143	0.11	15.873	0.04	5.71	0.08	11.43
benzoate	$C_7H_6O_2$	300	42.9	0.11	4.762	0.04	1.71	0.08	3.43
benzyl alcohol	C_7H_8O	20	2.86	0.11	0.317	0.04	0.11	0.16	0.46
benzaldehyde	C_7H_6O	2400	343	0.11	38.095	0.04	13.71	0.00	0.00
acetone	C_3H_6O	770	257	0.11	28.519	0.07	18.74	0.02	5.13
methyl acetate	$C_3H_6O_2$	870	2.9	0.11	0.322	0.24	0.70	0.19	0.56
tert-butanol	$C_4H_{10}O$	0.04	0.01	0.11	0.001	0.24	0.00	0.19	0.00
alanine	$C_3H_7O_2N$	1.2	0.40	0.11	0.044	0.24	0.10	0.19	0.08
			$\Sigma_i\alpha_i$ or $\Sigma_i\alpha_i k_i$	1.00	8.8×10^8 $M_C^{-1}s^{-1}$	1.00	4.08×10^8 $M_C^{-1}s^{-1}$	1.00	2.11×10^8 $M_C^{-1}s^{-1}$

[a]Rate constants obtained from the NDRL/NIST solution kinetics database (kinetics.nist.gov/solution/).[67]

https://doi.org/10.1021/acs.est.3c00909
Environ. Sci. Technol. 2023, 57, 7634−7643

will also screen incoming UV photons from being absorbed by the e_{aq}^- sensitizer (e.g., sulfite), thereby decreasing the rate of e_{aq}^- formation. Both e_{aq}^- scavenging and light screening by DOM will decrease the rate of e_{aq}^--mediated target contaminant degradation.[45,47] In ARP, where DOM is continuously exposed to e_{aq}^-, the light screening characteristics and e_{aq}^- scavenging likely change over time as e_{aq}^- reactions modify DOM structure. The k_{DOM,e_{aq}^-} values presented in Table 1, however, represent initial conditions before each DOM isolate has undergone transformation by e_{aq}^-.

To evaluate the impact of e_{aq}^- exposure on DOM light screening and e_{aq}^- scavenging, we performed an experiment in which 10 mM sodium sulfite was irradiated with low-pressure Hg vapor lamps (emitting at 254 nm) in the presence of 10 $mg_C\ L^{-1}$ SRNOM II. UV/sulfite experiments were conducted under anerobic conditions with a reactor pH ≥ 9.5 to minimize DOM's reaction with radical species other than e_{aq}^-.[16,45,56,57] Even though sulfite and sulfite radicals may directly react with DOM moieties, for simplicity it was assumed that DOM reacted predominantly with e_{aq}^- in the UV/sulfite system. However, it is not possible to categorically exclude DOM transformations by sulfite radicals. During a 24 h irradiation experiment, 20 μM chloroacetate (MCAA) was spiked at various time points to serve as an e_{aq}^- probe as demonstrated in our previous study.[47] The resulting first-order degradation rate constants for chloroacetate transformation were used to calculate the e_{aq}^- concentration ($[e_{aq}^-]_t$) and e_{aq}^- scavenging capacity ($k'_{S,t}$) for each chloroacetate spike time, t.

Results from chloroacetate spikes over a 24 h UV/sulfite experiment indicate that the light screening and e_{aq}^- scavenging of 10 $mg_C\ L^{-1}$ SRNOM II dissipate after ~4 h, resulting in an $[e_{aq}^-]_t$ that peaks at ~7 h (Figure 4, see SI Text S6 for additional details on calculations). The rate of e_{aq}^- formation ($R_{f,t}^{e_{aq}^-}$), which is a function of the fraction of light absorbed by sulfite, increases from 2.3×10^{-7} M s^{-1} at 0 h to 3.8×10^{-7} M s^{-1} at 4 h. At 0 h, the solution absorbance at 254 nm was 0.49 cm^{-1}, the calculated absorbance due to sulfite was 0.19 cm^{-1}, and the fraction of light absorbed by sulfite was 38%. At 4 h, the fraction of light absorbed by sulfite was nearly 100%. This indicates that by ~4 h e_{aq}^- reactions have completely attenuated the absorbance of SRNOM II at 254 nm and that the remaining absorbance is completely attributable to sulfite (see SI Figure S6). Furthermore, the $k'_{S,t}$value decreased rapidly during the first ~4 h of the UV/sulfite experiment. At 0 h, the measured $k'_{S,t}$ was 1.5×10^5 s^{-1}, which agrees well with the value calculated the k_{DOM,e_{aq}^-} value for SRNOM II in Table 1 [$(10\ mg_C\ L^{-1}) \times (1.73 \times 10^4\ L\ mg_C^{-1}\ s^{-1}) = 1.73 \times 10^5\ s^{-1}$]. By ~4 h, the measured $k'_{S,t}$ is consistent with the calculated $k'_{S,t}$ of 20 μM chloroacetate (2×10^4 s^{-1}), indicating that the $k'_{S,t}$ from SRNOM II has been completely abated. Taken together, the results indicate that both light screening and e_{aq}^- scavenging decrease the $[e_{aq}^-]_t$ in the UV/sulfite system available for contaminant abatement. These impacts are anticipated to be greater at higher DOM concentrations. For example, Ren et al. demonstrated sustained light screening in the UV/sulfite system over 24 h at an Aldrich humic acid concentration of 50 $mg_C\ L^{-1}$.[6] This may present a challenge for e_{aq}^--based treatment of waste streams like ion exchange resin, regeneration brine, and reverse osmosis concentrate where DOM concentrations are elevated.

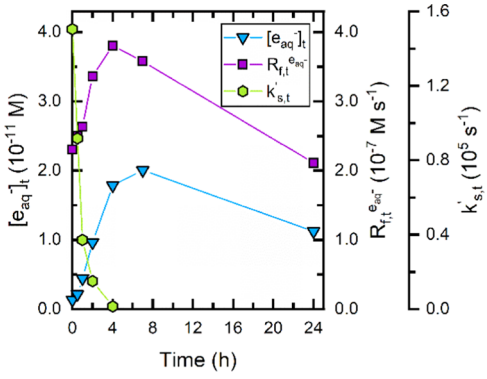

Figure 4. Photochemical parameters measured by chloroacetate for the UV/sulfite system in the presence of Suwanee River natural organic matter II (SRNOM II), including e_{aq}^- concentration ($[e_{aq}^-]_t$), formation rate ($R_{f,t}^{e_{aq}^-}$), and scavenging capacity ($k'_{S,t}$). SI Text S6 explains how these parameters were calculated. Experimental conditions: 10 W low-pressure Hg lamp, pH_0 = 9.5, 20 °C, 10 $mg_C\ L^{-1}$ $[SRNOM\ II]_0$, 10.4 mM $[sulfite]_0$, 20 μM $[MCAA]_0$ spikes, and 1.0 mM borate buffer in ultrapure water.

4. SIGNIFICANCE FOR HYDRATED ELECTRON-BASED CONTAMINANT DEGRADATION

ARP have received increasing attention for the destruction of recalcitrant chemical contaminants, most notably PFAS.[45,57,70,71] However, the role of DOM in these treatment technologies has not been adequately addressed.[45,57] Results from this study demonstrate that e_{aq}^- scavenging by DOM will significantly impact the rate of target contaminant degradation in ARP. We recommend that a k_{DOM,e_{aq}^-} value of 1.2×10^8 $M_C^{-1}\ s^{-1}$ (1.0×10^4 L $mg_C^{-1}\ s^{-1}$) be used to evaluate the e_{aq}^- scavenging impact of DOM in future studies. Given that k_{DOM,e_{aq}^-} values vary by a factor of 4, additional research is needed to develop structure-reactivity relationships to predict e_{aq}^- scavenging by DOM in different contexts.

Another implication of this research is that the increases in k_{DOM,e_{aq}^-} resulting from high ionic strength or alkaline pH, as observed in treating concentrated waste streams, are unlikely to significantly impact the efficiency of e_{aq}^--based treatment. We showed that increasing ionic strength from 0.02 to 0.12 M or increasing pH from 5 to 9 results in only a 1.5-fold increase in k_{DOM,e_{aq}^-}. On the other hand, increasing the DOM concentration from 10 to 100 $mg_C\ L^{-1}$ results in a 10-fold increase in the e_{aq}^- scavenging capacity in addition to a significant increase in UV photon screening. Thus, increases in DOM concentration in these waste streams will likely outweigh any increase in k_{DOM,e_{aq}^-} values that come from varying pH and ionic strength.

The temporal nature of the e_{aq}^- formation rate, scavenging capacity, and concentration demonstrated in Figure 4 indicates that e_{aq}^- scavenging by DOM is long-lived and has the potential to significantly impact ARP performance. The results shown in Figure 4 also raise several questions to be addressed in future research. First, we observed that the absorbance at 254 nm and e_{aq}^- scavenging capacity of DOM were completely attenuated at ~4 h of UV/sulfite treatment but [DOC] measured for samples collected at 2 and 24 h were the same within error of those measured at 0 h (SI Figure S9). This result indicates that the end products of e_{aq}^- reaction with DOM are not chromophoric (do not absorb at 254 nm) and

https://doi.org/10.1021/acs.est.3c00909
Environ. Sci. Technol. 2023, 57, 7634−7643

do not volatilize in our system, which was continuously sparged with nitrogen gas. Future research is needed to elucidate the composition of these products to explain the lack of change in [DOC] during UV/sulfite treatment. Second, future research should also investigate the impact of DOM in the sequential oxidation−reduction system described by Liu et al.[72] The oxidation step, which involves the formation of $^{\bullet}OH$ from heat-activated persulfate, will likely be impacted by DOM given the known reactivity of $^{\bullet}OH$ with DOM. While mineralization of DOM in this stage may alleviate e_{aq}^- scavenging by DOM in the subsequent reduction step, buildup of bicarbonate could negatively impact subsequent reductive treatment due to e_{aq}^- scavenging. Third, the temporal variation in e_{aq}^- photochemical parameters due to DOM modifications begs the question of how these parameters change in other photochemical treatment systems (i.e., UV-AOP). Although a prior study has evaluated this question and found minimal impacts under typical UV-AOP fluences (~1000 mJ cm^{-2}) using low-pressure Hg lamps,[73] more studies are warranted.

■ ASSOCIATED CONTENT

Supporting Information

The Supporting Information is available free of charge at https://pubs.acs.org/doi/10.1021/acs.est.3c00909.

List of chemicals used in this study; $SUVA_{254}$ and spectral slope calculations from DOM absorbance measurements; kinetic data for DOM-e_{aq}^- bimolecular rate constant determination; M_nQ calculations; SRNOM II irradiation in UV/sulfite system; and measured DOC concentration during 24 h experiment (PDF)

■ AUTHOR INFORMATION

Corresponding Authors

Stephen P. Mezyk − *Department of Chemistry and Biochemistry, California State University Long Beach, Long Beach, California 90840, United States*; Phone: 562.985.4649; Email: Stephen.Mezyk@csulb.edu

Garrett McKay − *Zachry Department of Civil & Environmental Engineering, Texas A&M University, College Station, Texas 77845, United States*; orcid.org/0000-0002-6529-0892; Phone: 979.458.6540; Email: gmckay@tamu.edu, @garrettjmckay

Authors

Benjamin D. Fennell − *Zachry Department of Civil & Environmental Engineering, Texas A&M University, College Station, Texas 77845, United States*; orcid.org/0000-0001-6525-5395

Douglas Fowler − *Department of Chemistry and Biochemistry, California State University Long Beach, Long Beach, California 90840, United States*

Complete contact information is available at: https://pubs.acs.org/10.1021/acs.est.3c00909

Notes

The authors declare no competing financial interest.

■ ACKNOWLEDGMENTS

The authors gratefully acknowledge support from the U.S. National Science Foundation (CBET #2050934, # 2050882). Thanks go to Dr. James Kiddle for help with conducting pulse radiolysis experiments. B.D.F. gratefully acknowledges financial support from the Texas A&M University Graduate Merit Fellowship, Stantec & AWWA Water Equation, and the Texas Engineering Foundation. The authors are thankful for the collaborative efforts at the Radiation Laboratory, which is supported by the Office of Basic Energy Sciences, U.S. Department of Energy.

■ REFERENCES

(1) Aiken, G. R.; McKnight, D. M.; Wershaw, R. L.; MacCarthy, P. *Humic Substances in Soil, Sediment, and Water*; John Wiley & Sons, Inc., 1985.

(2) Ulliman, S. L.; Miklos, D. B.; Hübner, U.; Drewes, J. E.; Linden, K. G. Improving UV/H_2O_2 Performance Following Tertiary Treatment of Municipal Wastewater. *Environ. Sci.: Water Res. Technol.* **2018**, *4*, 1321−1330.

(3) Rosenfeldt, E. J.; Linden, K. G.; Canonica, S.; von Gunten, U. Comparison of the Efficiency of ·OH Radical Formation During Ozonation and the Advanced Oxidation Processes O_3/H_2O_2 and UV/H_2O_2. *Water Res.* **2006**, *40*, 3695−3704.

(4) Li, X.; Fang, J.; Liu, G.; Zhang, S.; Pan, B.; Ma, J. Kinetics and Efficiency of the Hydrated Electron-induced Dehalogenation by the Sulfite/UV Process. *Water Res.* **2014**, *62*, 220−228.

(5) Wang, X.; Liu, H.; Shan, C.; Zhang, W.; Pan, B. A Novel Combined Process for Efficient Removal of Se(VI) from Sulfate-rich Water: Sulfite/UV/Fe(III) Coagulation. *Chemosphere* **2018**, *211*, 867−874.

(6) Ren, Z.; Bergmann, U.; Leiviska, T. Reductive Degradation of Perfluorooctanoic Acid in Complex Water Matrices by Using the UV/sulfite Process. *Water Res.* **2021**, *205*, No. 117676.

(7) Westerhoff, P.; Mezyk, S. P.; Cooper, W. J.; Minakata, D. Electron Pulse Radiolysis Determination of Hydroxyl Radical Rate Constants with Suwannee River Fulvic Acid and Other Dissolved Organic Matter Isolates. *Environ. Sci. Technol.* **2007**, *41*, 4640−4646.

(8) McKay, G.; Kleinman, J. L.; Johnston, K. M.; Dong, M. M.; Rosario-Ortiz, F. L.; Mezyk, S. P. Kinetics of the Reaction Between the Hydroxyl Radical and Organic Matter Standards from the International Humic Substance Society. *J. Soils Sediments* **2014**, *14*, 298−304.

(9) Lei, X.; Lei, Y.; Guan, J.; Westerhoff, P.; Yang, X. Kinetics and Transformations of Diverse Dissolved Organic Matter Fractions with Sulfate Radicals. *Environ. Sci. Technol.* **2022**, *56*, 4457−4466.

(10) Yan, S.; Liu, Y.; Lian, L.; Li, R.; Ma, J.; Zhou, H.; Song, W. Photochemical Formation of Carbonate Radical and its Reaction with Dissolved Organic Matters. *Water Res.* **2019**, *161*, 288−296.

(11) Lei, Y.; Lei, X.; Westerhoff, P.; Zhang, X.; Yang, X. Reactivity of Chlorine Radicals ($Cl^{\bullet}$ and $Cl_2^{\bullet-}$) with Dissolved Organic Matter and the Formation of Chlorinated Byproducts. *Environ. Sci. Technol.* **2021**, *55*, 689−699.

(12) Lei, Y.; Lei, X.; Westerhoff, P.; Tong, X.; Ren, J.; Zhou, Y.; Cheng, S.; Ouyang, G.; Yang, X. Bromine Radical ($Br^{\bullet}$ and $Br_2^{\bullet-}$) Reactivity with Dissolved Organic Matter and Brominated Organic Byproduct Formation. *Environ. Sci. Technol.* **2022**, *56*, 5189−5199.

(13) Li, X.; Ma, J.; Liu, G.; Fang, J.; Yue, S.; Guan, Y.; Chen, L.; Liu, X. Efficient Reductive Dechlorination of Monochloroacetic Acid by Sulfite/UV Process. *Environ. Sci. Technol.* **2012**, *46*, 7342−7349.

(14) Xie, B.; Li, X.; Huang, X.; Xu, Z.; Zhang, W.; Pan, B. Enhanced Debromination of 4-Bromophenol by the UV/Sulfite Process: Efficiency and Mechanism. *J. Environ. Sci.* **2017**, *54*, 231−238.

(15) Xiao, Q.; Wang, T.; Yu, S.; Yi, P.; Li, L. Influence of UV Lamp, Sulfur(IV) Concentration, and pH on Bromate Degradation in UV/Sulfite Systems: Mechanisms and Applications. *Water Res.* **2017**, *111*, 288−296.

(16) Buxton, G. V.; Greenstock, C. L.; Helman, W. P.; Ross, A. B. Critical Review of Rate Constants for Reactions of Hydrated Electrons, Hydrogen Atoms and Hydroxyl Radicals (·OH/·O^-) in Aqueous Solution. *J. Phys. Chem. Ref. Data* **1988**, *17*, 513−886.

(17) Botlaguduru, V. S. V.; Batchelor, B.; Abdel-Wahab, A. Application of UV−Sulfite Advanced Reduction Process to Bromate Removal. *J. Water Process Eng.* **2015**, *5*, 76−82.
(18) Liu, X.; Wang, L.; Sun, Z.; Shao, Y.; Yu, T. Treatment of Aqueous Bromate by Superparamagnetic BiOCl-Mediated Advanced Reduction Process. *Catalysts* **2017**, *7*, No. 131.
(19) Nawaz, S.; Shah, N. S.; Khan, J. A.; Sayed, M.; Al-Muhtaseb, A. a. H.; Andersen, H. R.; Muhammad, N.; Murtaza, B.; Khan, H. M. Removal Efficiency and Economic Cost Comparison of Hydrated Electron-mediated Reductive Pathways for Treatment of Bromate. *Chem. Eng. J.* **2017**, *320*, 523−531.
(20) Jung, B.; Nicola, R.; Batchelor, B.; Abdel-Wahab, A. Effect of Low- and Medium-pressure Hg UV Irradiation on Bromate Removal in Advanced Reduction Process. *Chemosphere* **2014**, *117*, 663−672.
(21) Xiao, Q.; Yu, S.; Li, L.; Wang, T.; Liao, X.; Ye, Y. An Overview of Advanced Reduction Processes for Bromate Removal from Drinking Water: Reducing Agents, Activation Methods, Applications and Mechanisms. *J. Hazard. Mater.* **2017**, *324*, 230−240.
(22) Xiao, Q.; Yu, S.; Li, L.; Zhang, Y.; Yi, P. Degradation of Bromate by Fe(II)Ti(IV) Layered Double Hydroxides Nanoparticles Under Ultraviolet Light. *Water Res.* **2019**, *150*, 310−320.
(23) Yu, K.; Li, X.; Chen, L.; Fang, J.; Chen, H.; Li, Q.; Chi, N.; Ma, J. Mechanism and Efficiency of Contaminant Reduction by Hydrated Electron in the Sulfite/Iodide/UV Process. *Water Res.* **2018**, *129*, 357−364.
(24) Liu, X.; Zhong, J.; Fang, L.; Wang, L.; Ye, M.; Shao, Y.; Li, J.; Zhang, T. Trichloroacetic Acid Reduction by an Advanced Reduction Process Based on Carboxyl Anion Radical. *Chem. Eng. J.* **2016**, *303*, 56−63.
(25) Liu, X.; Yoon, S.; Batchelor, B.; Abdel-Wahab, A. Degradation of Vinyl Chloride (VC) by the Sulfite/UV Advanced Reduction Process (ARP): Effects of Process Variables and a Kinetic Model. *Sci. Total Environ.* **2013**, *454-455*, 578−583.
(26) Liu, X.; Yoon, S.; Batchelor, B.; Abdel-Wahab, A. Photochemical Degradation of Vinyl Chloride with an Advanced Reduction Process (ARP) − Effects of Reagents and pH. *Chem. Eng. J.* **2013**, *215−216*, 868−875.
(27) Wentworth, W. E.; Becker, R. S.; Tung, R. Thermal Electron Attachment to Some Aliphatic and Aromatic Chloro, Bromo, and Iodo Derivatives. *J. Phys. Chem. A* **1967**, *71*, 1652−1665.
(28) Sun, C.; Chang, W.; Ma, W.; Chen, C.; Zhao, J. Photoreductive Debromination of Decabromodiphenyl Ethers in the Presence of Carboxylates Under Visible Light Irradiation. *Environ. Sci. Technol.* **2013**, *47*, 2370−2377.
(29) Yu, X.; Cabooter, D.; Dewil, R. Effects of Process Variables and Kinetics on the Degradation of 2,4-Dichlorophenol Using Advanced Reduction Processes (ARP). *J. Hazard. Mater.* **2018**, *357*, 81−88.
(30) Yazdanbakhsh, A.; Eslami, A.; Moussavi, G.; Rafiee, M.; Sheikhmohammadi, A. Photo-assisted Degradation of 2, 4, 6-Trichlorophenol by an Advanced Reduction Process Based on Sulfite Anion Radical: Degradation, Dechlorination and Mineralization. *Chemosphere* **2018**, *191*, 156−165.
(31) Shoute, L. C. T.; Mittal, J. P.; Neta, P. Reduction and Defluorination of Pentafluorophenol in Aqueous Solutions. *J. Phys. Chem. B* **1996**, *100*, 3016−3019.
(32) Qu, Y.; Zhang, C.; Li, F.; Chen, J.; Zhou, Q. Photo-reductive Defluorination of Perfluorooctanoic Acid in Water. *Water Res.* **2010**, *44*, 2939−2947.
(33) Song, Z.; Tang, H.; Wang, N.; Zhu, L. Reductive Defluorination of Perfluorooctanoic Acid by Hydrated Electrons in a Sulfite-mediated UV Photochemical System. *J. Hazard. Mater.* **2013**, *262*, 332−338.
(34) Gu, Y.; Liu, T.; Wang, H.; Han, H.; Dong, W. Hydrated Electron Based Decomposition of Perfluorooctane Sulfonate (PFOS) in the VUV/Sulfite System. *Sci. Total Environ.* **2017**, *607-608*, 541−548.
(35) Tian, H.; Gao, J.; Li, H.; Boyd, S. A.; Gu, C. Complete Defluorination of Perfluorinated Compounds by Hydrated Electrons Generated from 3-Indole-Acetic-Acid in Organomodified Montmorillonite. *Sci. Rep.* **2016**, *6*, No. 32949.
(36) Tian, H.; Gu, C. Effects of Different factors on Photodefluorination of Perfluorinated Compounds by Hydrated Electrons in Organo-montmorillonite System. *Chemosphere* **2018**, *191*, 280−287.
(37) Chen, Z.; Mi, N.; Li, C.; Teng, Y.; Chen, Y.; Gu, C. Effects of Different Variables on Photodestruction of Perfluorooctanoic Acid in Self-assembled Micelle System. *Sci. Total Environ.* **2020**, *742*, No. 140438.
(38) Chen, Z.; Li, C.; Gao, J.; Dong, H.; Chen, Y.; Wu, B.; Gu, C. Efficient Reductive Destruction of Perfluoroalkyl Substances under Self-Assembled Micelle Confinement. *Environ. Sci. Technol.* **2020**, *54*, 5178−5185.
(39) Chen, Z.; Teng, Y.; Mi, N.; Jin, X.; Yang, D.; Wang, C.; Wu, B.; Ren, H.; Zeng, G.; Gu, C. Highly Efficient Hydrated Electron Utilization and Reductive Destruction of Perfluoroalkyl Substances Induced by Intermolecular Interaction. *Environ. Sci. Technol.* **2021**, *55*, 3996−4006.
(40) Bentel, M. J.; Yu, Y.; Xu, L.; Li, Z.; Wong, B. M.; Men, Y.; Liu, J. Defluorination of Per- and Polyfluoroalkyl Substances (PFASs) with Hydrated Electrons: Structural Dependence and Implications to PFAS Remediation and Management. *Environ. Sci. Technol.* **2019**, *53*, 3718−3728.
(41) Bentel, M. J.; Yu, Y.; Xu, L.; Kwon, H.; Li, Z.; Wong, B. M.; Men, Y.; Liu, J. Degradation of Perfluoroalkyl Ether Carboxylic Acids with Hydrated Electrons: Structure-Reactivity Relationships and Environmental Implications. *Environ. Sci. Technol.* **2020**, *54*, 2489−2499.
(42) Liu, C. J.; McKay, G.; Jiang, D.; Tenorio, R.; Cath, J. T.; Amador, C.; Murray, C. C.; Brown, J. B.; Wright, H. B.; Schaefer, C.; Higgins, C. P.; Bellona, C.; Strathmann, T. J. Pilot-Scale Field Demonstration of a Hybrid Nanofiltration and UV-Sulfite Treatment Train for Groundwater Contaminated by Per- and Polyfluoroalkyl Substances (PFASs). *Water Res.* **2021**, *205*, No. 117677.
(43) Cui, J.; Deng, Y. Hydrated Electron Degradation of PFOA Laden on Ion-Exchange Resins in the Presence of Natural Organic Matter. *ACS ES&T Eng.* **2022**, 86−93.
(44) Duan, Y.; Batchelor, B. Impacts of Natural Organic Matter on Perchlorate Removal by an Advanced Reduction Process. *J. Environ. Sci. Health, Part A* **2014**, *49*, 731−740.
(45) Fennell, B. D.; Mezyk, S. P.; McKay, G. Critical Review of UV-Advanced Reduction Processes for the Treatment of Chemical Contaminants in Water. *ACS Environ. Au* **2022**, *2*, 178−205.
(46) What are Humic Substances?. https://humic-substances.org/. (accessed October 5, 2021).
(47) Fennell, B. D.; Odorisio, A.; McKay, G. Quantifying Hydrated Electron Transformation Kinetics in UV-Advanced Reduction Processes Using the $R_{e^-,UV}$ Method. *Environ. Sci. Technol.* **2022**, *56*, 10329−10338.
(48) Humphrey, R. E.; Ward, M. H.; Hinze, W. Spectrophotometric Determination of Sulfite with 4,4′-Dithiodipyridine and 5,5′-Dithiobis-(2-Nitrobenzoic Acid). *Anal. Chem.* **1970**, *42*, 698−702.
(49) Whitham, K.; Lyons, S.; Miller, R.; Nett, D.; Treas, P.; Zante, A.; Fessenden, R. W.; Thomas, M. D.; Wang, Y. In *Linear Accelerator for Radiation Chemistry Research at Notre Dame*, Proceedings Particle Accelerator Conference; IEEE: Dallas, TX, USA, 1995; pp 131−133.
(50) Jeong, J.; Song, W.; Cooper, W. J.; Jung, J.; Greaves, J. Degradation of Tetracycline Antibiotics: Mechanisms and Kinetic Studies for Advanced Oxidation/Reduction Processes. *Chemosphere* **2010**, *78*, 533−540.
(51) Keen, O. S.; McKay, G.; Mezyk, S. P.; Linden, K. G.; Rosario-Ortiz, F. L. Identifying the Factors that Influence the Reactivity of Effluent Organic Matter with Hydroxyl Radicals. *Water Res.* **2014**, *50*, 408−419.
(52) Dong, M. M.; Mezyk, S. P.; Rosario-Ortiz, F. L. Reactivity of Effluent Organic Matter (EfOM) with Hyroxyl Radical as a Function of Molecular Weight. *Environ. Sci. Technol.* **2010**, *44*, 5714−5720.

https://doi.org/10.1021/acs.est.3c00909
Environ. Sci. Technol. 2023, 57, 7634−7643

(53) Rickman, K. A.; Mezyk, S. P. Kinetics and Mechanisms of Sulfate Radical Oxidation of β-lactam Antibiotics in Water. *Chemosphere* **2010**, *81*, 359−365.
(54) Cole, S. K.; Cooper, W. J.; Fox, R. V.; Gardinali, P. R.; Mezyk, S. P.; Mincher, B. J.; O'Shea, K. E. Free Radical Chemistry of Disinfection Byproducts. 2. Rate Constants and Degradation Mechanisms of Trichloronitromethane (Chloropicrin). *Environ. Sci. Technol.* **2007**, *41*, 863−869.
(55) Elemental Compositions and Stable Isotopic Ratios of IHSS Samples. https://humic-substances.org/elemental-compositions-and-stable-isotopic-ratios-of-ihss-samples/. (accessed March 30, 2022).
(56) Maza, W. A.; Breslin, V. M.; Plymale, N. T.; DeSario, P. A.; Epshteyn, A.; Owrutsky, J. C.; Pate, B. B. Nanosecond Transient Absorption Studies of the pH-dependent Hydrated Electron Quenching by HSO_3^-. *Photochem. Photobiol. Sci.* **2019**, *18*, 1526−1532.
(57) Cui, J.; Gao, P.; Deng, Y. Destruction of Per- and Polyfluoroalkyl Substances (PFAS) with Advanced Reduction Processes (ARPs): A Critical Review. *Environ. Sci. Technol.* **2020**, *54*, 3752−3766.
(58) Jin, S.; Mofidi, A. A.; Linden, K. G. Polychromatic UV Fluence Measurement Using Chemical Actinometry, Biodosimetry, and Mathematical Techniques. *J. Environ. Eng.* **2006**, *132*, 831−841.
(59) Beltran, F. J.; Ovejero, G.; Garcia-Araya, J. F.; Rivas, J. Oxidation of Polynuclear Aromatic Hydrocarbons in Water. 2. UV Radiation and Ozonation in the Presence of UV Radiation. *Ind. Eng. Chem. Res.* **1995**, *34*, 1607−1615.
(60) Crittenden, J. C.; Hu, S.; Hand, D. W.; Green, S. A. A Kinetic Model for H_2O_2/UV Process In a Completely Mixed Batch Reactor. *Water Res.* **1999**, *33*, 2315−2328.
(61) Ritchie, J. D.; Perdue, E. M. Proton-binding Study of Standard and Reference Fulvic Acids, Humic Acids, and Natural Organic Matter. *Geochim. Cosmochim. Acta* **2003**, *67*, 85−96.
(62) Avena, M. J.; Vermeer, A. W. P.; Koopal, L. K. Volume and Structure of Humic Acids Studies by Viscometry pH and Electrolyte Concentration Effects. *Colloids Surf., A* **1999**, *151*, 213−224.
(63) Green, S. A.; Morel, F. M. M.; Blough, N. V. Investigation of Electrostatic Properties of Humic Substances by Fluorescence Quenching. *Environ. Sci. Technol.* **1992**, *26*, 294−302.
(64) Li, H.; McKay, G. Relationships between the Physicochemical Properties of Dissolved Organic Matter and Its Reaction with Sodium Borohydride. *Environ. Sci. Technol.* **2021**, *55*, 10843−10851.
(65) Acidic Functional Groups of IHSS Samples. https://humic-substances.org/acidic-functional-groups-of-ihss-samples/. (accessed March 30, 2022).
(66) ^{13}C NMR Estimates of Carbon Distribution. https://humic-substances.org/13c-nmr-estimates-of-carbon-distribution-in-ihss-samples/. (accessed March 30, 2022).
(67) *NDRL/NIST Solution Kinetics Database on the Web*. 2002 ed.; National Institute of Standards and Technology: Notre Dame Radiation Laboratory, 2023.
(68) Aeschbacher, M.; Graf, C.; Schwarzenbach, R. P.; Sander, M. Antioxidant Properties of Humic Substances. *Environ. Sci. Technol.* **2012**, *46*, 4916−4925.
(69) Rosario-Ortiz, F. L.; Mezyk, S.; Doud, D. F. R.; Snyder, S. A. Quantitative Correlation of Absolute Hydroxyl Radical Rate Constants with Non-Isolated Effluent Organic Matter Bulk Properties in Water. *Environ. Sci. Technol.* **2008**, *42*, 5924−5930.
(70) Alalm, M. G.; Boffito, D. C. Mechanisms and Pathways of PFAS Degradation by Advanced Oxidation and Reduction Processes: A Critical Review. *Chem. Eng. J.* **2022**, *450*, No. 138352.
(71) Liu, F.; Guan, X.; Xiao, F. Photodegradation of Per- and Polyfluoroalkyl Substances in Water: A Review of Fundamentals and Applications. *J. Hazard. Mater.* **2022**, *439*, No. 129580.
(72) Liu, Z.; Bentel, M. J.; Yu, Y.; Ren, C.; Gao, J.; Pulikkal, V. F.; Sun, M.; Men, Y.; Liu, J. Near-Quantitative Defluorination of Perfluorinated and Fluorotelomer Carboxylates and Sulfonates with Integrated Oxidation and Reduction. *Environ. Sci. Technol.* **2021**, *55*, 7052−7062.
(73) Vinge, S. L.; Shaheen, S. W.; Sharpless, C. M.; Linden, K. G. Nitrate with Benefits: Optimizing Radical Production During UV Water Treatment. *Environ. Sci.: Water Res. Technol.* **2020**, *6*, 1163−1175.

https://doi.org/10.1021/acs.est.3c00909
Environ. Sci. Technol. 2023, 57, 7634−7643